Phys Chem Minerals (1991) 17:591–603

PHYSICS AND CHEMISTRY OF MINERALS

Paraelectric-Antiferroelectric Phase Transition in Titanite, $CaTiSiO_5$

I. A High Temperature X-ray Diffraction Study of the Order Parameter and Transition Mechanism

Subrata Ghose [1], Yoshiaki Ito [1], and Dorian M. Hatch [2]

[1] Mineral Physics Group, Department of Geological Sciences, University of Washington, Seattle, WA 98195, USA
[2] Department of Physics, Brigham Young University, Provo, UT 84602, USA

Received April 1, 1990

Abstract. The paraelectric to antiferroelectric phase transition in titanite at ~500 K involves a displacement of the titanium atom from the center of the $[TiO_6]$ octahedron in the paraelectric phase ($A2/a$) to an off-center position in the antiferroelectric ($P2_1/a$) phase. We have carried out a detailed single crystal high temperature x-ray diffraction study of the phase transition including structure refinements at 294, 350, 400, 430, 440, 450, 500, 600, and 700 K. The unit cell dimensions show a pronounced hysteresis effect in the 450–500 K range on heating and cooling during the first cycle along with a reduction of the transition temperature, T_c from 495 ±5 K on heating to 445±5 K on cooling. The hysteresis effect disappears on further heating and the superstructure reflections show residual intensities above T_c (445 K). An order parameter treatment of the phase transition is presented in terms of Landau theory and induced representation theory. The Ti-displacements parallel and antiparallel to **a** are taken as the primary order parameter η, which transforms as the Y_2^+ representation. A coupling of Y_2^+ with Γ_1^+ results in the linear-quadratic coupling of the spontaneous strain components, ε_{ij} with η. The Ti-displacements are coupled linearly to the Ca-displacements. Both sets of displacements predicted from induced representation theory are observed experimentally. The phase transition is initially driven by the soft mode at the zone boundary point Y_2^+; near T_c critical fluctuations set in and an order-disorder mechanism finally drives the phase transition, whereby parallel and antiparallel Ti-displacements related by [0, 1/2, 1/2] in adjacent domains are dynamically interchanged. Immediately above T_c, the high temperature ($A2/a$) phase is a statistical average of small dynamic antiphase domains of the low temperature ($P2_1/a$) phase. Vacancies and defects pinning the domain boundaries may drastically alter the transition behavior and affect the domain mobility.

Introduction

Titanite, $CaTiSiO_5$, belongs to the group of ferroelectric and antiferroelectric titanates (e.g. $BaTiO_3$) where the electric polarization results from the displacement of the titanium atom from the center of the $[TiO_6]$ octahedron. Titanite, also known as sphene because of its common sphenoidal (wedge-shaped) habit, is a common accessory mineral with monoclinic symmetry in a variety of metamorphic and igneous rocks. Natural titanites usually show a coupled chemical substitution of the type $Ti^{4+} + O^{2-} \rightleftharpoons (Fe^{3+}, Al^{3+}) + (F^-, OH^-)$. Pure titanite has been synthesized by heating a mixture of the relevant oxides in a crucible above the melting point (1382° C) and slowly cooling the melt. Single crystals have been grown by the Czochralski (Brower and Robbins 1969), hydrothermal (Franke and Ghobarkar 1980) and floating zone (Tanaka et al. 1988) methods. At room temperature pure synthetic titanite and natural titanites with less than 3–4 mol% substitution of Ti have the space group $P2_1/a$, whereas those with more than 20 mol% substitution have the space group $A2/a$ (Robbins 1968; Speer and Gibbs 1976; Higgins and Ribbe 1976). Using a high temperature single crystal x-ray diffraction technique Taylor and Brown (1976) showed that pure titanite undergoes a reversible displacive phase transition from $P2_1/a$ to $A2/a$ at 220±20° C. This transition has also been confirmed by high temperature dielectric measurements (Tanaka et al. 1988), the reported transition temperature being 235° C. The crystal structure of a natural titanite (space group $C2/c$) was first determined by Zachariasen (1930). It consists of corner-sharing $[TiO_6]$ octahedral chains cross-linked by isolated tetrahedral $[SiO_4]$ groups and Ca^{2+} ions in an irregular seven-fold coordination. The structure was subsequently refined by Mongiorgi and Sanseverino (1968), who chose a different unit cell (space group $A2/a$). The crystal structure of the low temperature phase of pure titanite (space group

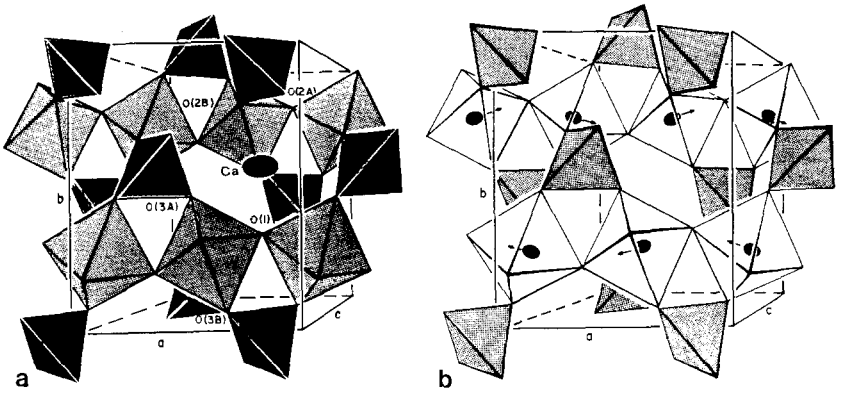

Fig. 1. (**a**) A view of the titanite structure showing the zigzag chain of Ti-octahedra cross-linked by isolated Si-tetrahedra. One of the Ca-position is shown (after Taylor and Brown 1976). (**b**) A view of the titanite structure showing the Ti-displacements parallel and antiparallel to **a** in adjacent octahedral chains (after Taylor and Brown 1976)

$P2_1/a$) was determined by Speer and Gibbs (1976) and Taylor and Brown (1976). They found the titanium atom to be displaced from the center of the octahedron closer to one of the apical oxygens (O1). The titanium displacements in adjacent octahedral chains are parallel and antiparallel to **a**, thus giving rise to an antiferroelectric arrangement of the electric polarization vectors in the low temperature phase (Fig. 1). From structure refinements of a pure synthetic titanite at various temperatures above and below the transition, Taylor and Brown (1976) showed that the Ti displacement decreases with increasing temperature as T approaches T_c; above T_c, the titanium atom occupies the center of the $[TiO_6]$ octahedron. Above the transition, they found the major axis of the thermal vibration ellipsoid of titanium to be aligned parallel to the O(1)–Ti–O(1) bond with a root mean square displacement of 0.137 Å at 270° C. Although this displacement was found to be somewhat larger than that of Ti from the center of the octahedron in the low temperature phase, they could not settle the question whether the titanium position in the high temperature phase represents an average of two or more titanium positions or a single titanium position with a large thermal component in the axial direction of the octahedron. With a desire to settle this question and to precisely characterize the titanium displacements as a function of temperature and relate these displacements to the primary order parameter as well as the associated spontaneous strain, we have undertaken a detailed single crystal high temperature x-ray diffraction study of pure synthetic titanite. In this paper, we present our experimental results along with a generalized Landau symmetry description of the transition. We show that the transition is weakly first-order; it is initially driven by a soft phonon mode (Y_2^+) at the zone boundary, followed by an order-disorder mechanism near T_c. The dynamical characteristics of the phase transition are very similar to those observed for the $P\bar{1}-I\bar{1}$ transition in anorthite, $CaAl_2Si_2O_8$, at 516 K (Ghose et al. 1988; Van Tendeloo et al. 1989; Hatch and Ghose 1989).

Sample

Pure synthetic titanite was crystallized from a mixture of high purity oxides heated at 1150° C for 5 weeks in a platinum crucible by D.A. Hewitt, Virginia Polytechnic Institute and State University, Blacksburg, Virginia. A small portion of this sample was obtained through the courtesy of J.A. Speer, North Carolina State University, Raleigh, North Carolina, for our high temperature x-ray diffraction experiments. It is the same sample used by Speer and Gibbs (1976) and Taylor and Brown (1976). From a microprobe analysis, Higgins and Ribbe (1976) report about 3 percent deficiency in calcium with respect to five oxygens in the formula unit. The Ca^{2+} vacancies, if real, imply an equal number of O^{2-} vacancies as well.

Experimental Methods and Results

A single crystal sphere (diameter 0.25 mm) was prepared using a Bond-type sphere grinder (Bond 1951). All x-ray diffraction measurements were made on a large (Huber 512) four-circle x-ray diffractometer (chi-circle diameter 520 mm) with 2.4 kw MoK_α radiation. The diffractometer is automated using electronics and computer programs developed by Prof. C.L. Strouse, University of California at Los Angeles. A gas flow furnace with a temperature stability of ± 5 K capable of reaching 1100 K was used for the high temperature experiments (Tsukimura et al. 1989). The furnace was mounted on a $x-y-z$ stage directly across from the goniometer cradle which is offset by 63.5 mm from the chi-circle plane. This stage allows a precise positioning of the furnace with respect to the crystal which was mounted on a Pt/Pt–Rh thermocouple enclosed in a quartz capillary. The gas (air) flow was regulated through a flow valve at the rate of 1.5 l/min. The temperature calibration was carried out from the known thermal expansion of NaCl (Enck and Dommel 1965).

The unit cell dimensions were measured by least square refinement of 2θ values of 26 reflections within the 2θ range 35–45° at temperature intervals of 10 K (340–530 K) and 20 K (560–700 K) on heating and 20 K (320–400 K) and 5 K (435–495 K) on cooling (Fig. 2) during the first cycle. The unit cell dimensions were redetermined at 294, 350, 400, 430, 440, 450, 500, 600, and 700 K (av. of 5–9 measurements after every 3 hours) (Table 1, Fig. 3) during the second heating cycle. The intensities and line-widths of three superstructure reflections (401, 801, $\bar{4}01$) using $\theta-2\theta$ scans were monitored during the first cycle of heating and cooling through T_c (Fig. 5). The x-ray intensity data were measured up to $2\theta=65°$ with a scan speed of 3°/min (50 kV, 25 mA). The intensity

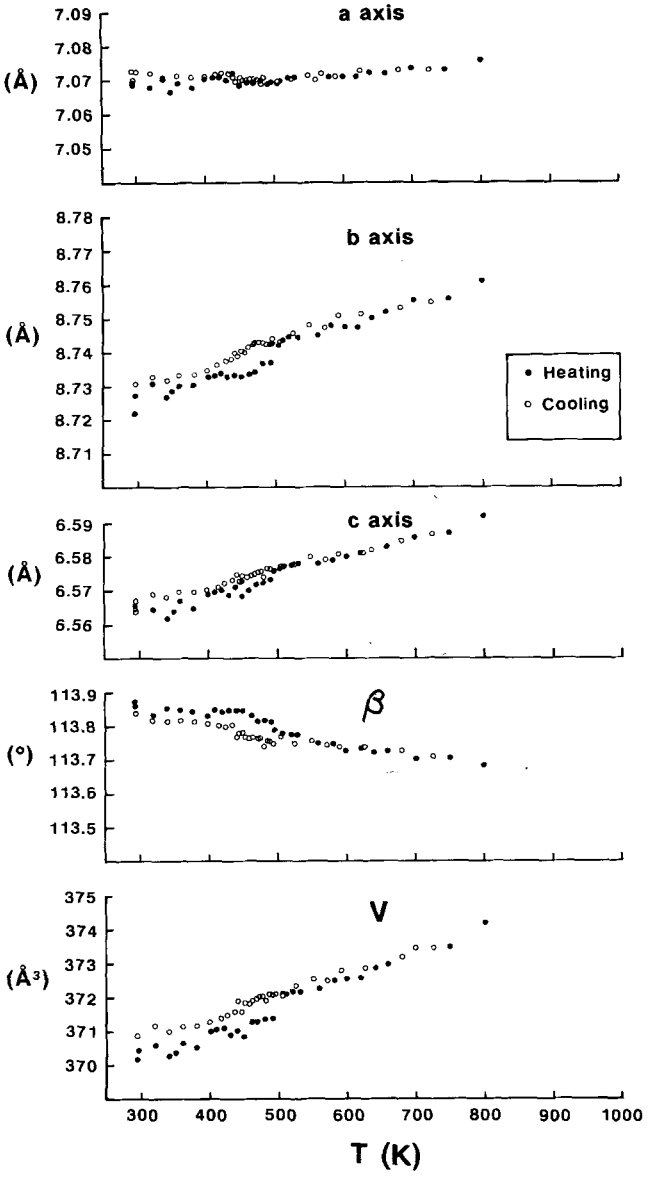

Fig. 2. The unit cell dimensions a, b, c, β, and volume V as a function of temperature on heating (●) and cooling (○) during the first cycle

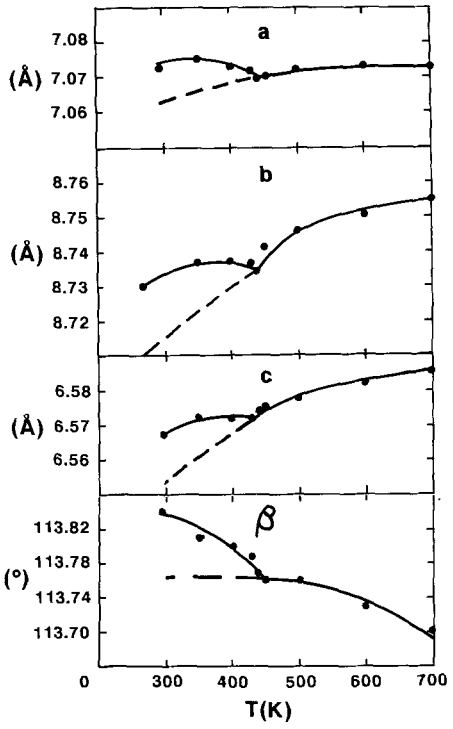

Fig. 3. Unit cell dimensions as a function of temperature on heating during the second cycle. The broken line indicates extrapolation below T_c, of high temperature thermal expansion behavior above T_c

data were corrected for absorption, Lorentz, and polarization factors. Least square refinements were carried out using a full matrix least-squares program (UPALS, Lundgren 1979) and anisotropic temperature factors. The atomic scattering factors including anomalous dispersion for Ca, Ti, Si, and O were taken from *International Tables for X-ray Crystallography*, v. IV (1974). The initial atomic positional coordinates were taken from Taylor and Brown (1976) for refinement of the structure of the low temperature phase ($P2_1/a$). A new origin at [0, −1/4, −1/4] was used for refinement of the high temperature $A2/a$ structure. Thus, a translation of [0, 1/4, 1/4] was added to these coordinates to obtain the input parameters for refinement of the $A2/a$ phase. Note that this necessary translation is not shown in Table 4 of Taylor and Brown (1976). The unit cell dimensions used for the structure refinements, intensity statistics and R-factors are listed in Table 1. The final atomic positional and thermal parameters are listed in Table 2 interatomic distances and angles in Table 3a, b, and a list of observed and calculated structure factors in Table 4.[1] The average standard deviations in Ca−O, Ti−O, and Si−O bond lengths are ±0.002, and in O−Ti−O and O−Si−O bond angles ±0.01°.

Thermal Expansion

The unit cell dimensions measured on heating and cooling from 294 to 800 K during the first cycle are plotted in Fig. 2. A thermal hysteresis in the 450–500 K range is clearly indicated: b and β show a negative and positive deviation respectively on heating and cooling with respect to the extrapolated values of the high temperature data above T_c. In particular, on heating the b dimension shows a small break near T_c, whereas all other unit cell dimensions are continuous on cooling. This hysteresis disappears on heating during the second cycle, where the unit cell dimensions follow essentially the same trend (Fig. 3) found on cooling during the first-cycle (Fig. 2).

Symmetry Analysis of the Transition

The symmetry aspects of the phase transition will now be discussed. A great deal of information concerning the

[1] For deposit

Table 1. Crystal data: synthetic titanite, $CaTiSiO_5$, as a function of temperature

	294 K	350 K	400 K	430 K	440 K	450 K	500 K	600 K	700 K
a (Å):	7.0722 (5)	7.0746 (4)	7.0730 (5)	7.0715 (5)	7.0701 (5)	7.0706 (5)	7.0719 (5)	7.0730 (5)	7.0726 (9)
b (Å):	8.7302 (7)	8.7373 (5)	8.7374 (6)	8.7365 (6)	8.7405 (7)	8.7416 (7)	8.7464 (7)	8.7508 (7)	8.7558 (11)
c (Å):	6.5672 (5)	6.5723 (4)	6.5716 (4)	6.5717 (4)	6.5747 (5)	6.5751 (5)	6.5783 (5)	6.5824 (5)	6.5859 (9)
β (°):	113.840 (2)	113.811 (2)	113.804 (2)	113.788 (2)	113.773 (2)	113.768 (2)	113.751 (2)	113.729 (2)	113.699 (3)
V (Å^3):	370.875	371.674	371.574	371.508	371.818	371.928	372.430	372.971	373.447
Space group:	$P2_1/a$	$P2_1/a$	$P2_1/a$	$P2_1/a$	$P2_1/a$	$P2_1/a$	$A2/a$	$A2/a$	$A2/a$
No. of refl.:	931	905	864	803	660	640	558	553	556
R:	0.034	0.030	0.030	0.028	0.030	0.028	0.028	0.032	0.033
R_w:	0.038	0.032	0.033	0.029	0.033	0.026	0.032	0.037	0.043

Table 2. Titanite, $CaTiSiO_5$: Atomic positional parameters and anisotropic thermal vibration parameters ($\beta_{ij} \times 10^5$) as a function of temperature

294 K

	Ca	Ti	Si	01	02A	02B	03A	03B
x	0.2421 (2)	0.5137 (1)	0.7483 (2)	0.7494 (5)	0.9097 (4)	0.0881 (4)	0.3829 (4)	0.6191 (4)
y	0.4185 (1)	0.2540 (1)	0.4327 (1)	0.3219 (2)	0.3161 (3)	0.1849 (3)	0.4609 (3)	0.0399 (3)
z	0.2511 (2)	0.7496 (1)	0.2491 (2)	0.7491 (6)	0.4332 (5)	0.0644 (5)	0.6456 (5)	0.8532 (5)
β_{11}	1135 (49)	574 (35)	282 (52)	337 (44)	602 (55)	561 (56)	569 (57)	541 (57)
β_{22}	196 (21)	194 (16)	87 (25)	241 (22)	293 (29)	298 (29)	155 (28)	156 (28)
β_{33}	375 (42)	246 (28)	102 (49)	554 (44)	239 (62)	300 (56)	496 (67)	670 (70)
β_{12}	0 (38)	34 (28)	15 (42)	23 (38)	54 (34)	28 (34)	87 (32)	76 (32)
β_{13}	−30 (38)	73 (24)	34 (44)	183 (38)	83 (47)	90 (48)	197 (51)	274 (53)
β_{23}	5 (39)	−34 (25)	32 (45)	11 (46)	32 (35)	25 (36)	97 (35)	138 (37)

350 K

	Ca	Ti	Si	01	02A	02B	03A	03B
x	0.2429 (2)	0.5127 (1)	0.7485 (2)	0.7488 (4)	0.9103 (4)	0.0881 (4)	0.3829 (4)	0.6187 (4)
y	0.4186 (1)	0.2536 (1)	0.4327 (1)	0.3213 (2)	0.3159 (3)	0.1848 (3)	0.4610 (3)	0.0399 (3)
z	0.2513 (2)	0.7496 (1)	0.2491 (2)	0.7491 (6)	0.4343 (4)	0.641 (4)	0.6463 (4)	0.8527 (4)
β_{11}	1219 (18)	429 (10)	282 (16)	378 (39)	646 (49)	656 (50)	585 (48)	537 (47)
β_{22}	193 (6)	183 (5)	95 (8)	231 (18)	299 (25)	290 (25)	208 (25)	188 (24)
β_{33}	499 (13)	343 (9)	223 (15)	835 (42)	298 (66)	376 (68)	637 (70)	610 (69)
β_{12}	19 (12)	28 (8)	−4 (13)	41 (33)	18 (31)	40 (31)	99 (30)	96 (29)
β_{13}	−37 (12)	101 (7)	68 (13)	300 (34)	82 (46)	167 (47)	301 (49)	256 (47)
β_{23}	6 (13)	4 (7)	−2 (14)	24 (44)	−7 (34)	20 (35)	122 (34)	82 (34)

400 K

	Ca	Ti	Si	01	02A	02B	03A	03B
x	0.2438 (2)	0.5114 (1)	0.7488 (2)	0.7487 (5)	0.9102 (4)	0.0879 (4)	0.3829 (4)	0.6184 (4)
y	0.4187 (1)	0.2533 (1)	0.4327 (1)	0.3213 (2)	0.3160 (4)	0.1848 (4)	0.4606 (3)	0.0395 (3)
z	0.2511 (3)	0.7497 (1)	0.2493 (3)	0.7481 (7)	0.4346 (5)	0.0639 (5)	0.6466 (5)	0.8524 (5)
β_{11}	1300 (44)	599 (27)	270 (44)	388 (39)	733 (52)	665 (52)	648 (52)	662 (52)
β_{22}	227 (18)	236 (14)	83 (22)	250 (20)	337 (31)	320 (31)	238 (30)	197 (29)
β_{33}	657 (39)	386 (25)	271 (44)	942 (44)	252 (69)	518 (76)	663 (82)	611 (81)
β_{12}	−17 (41)	40 (23)	19 (43)	−12 (37)	34 (34)	19 (34)	66 (33)	91 (32)
β_{13}	−39 (34)	106 (20)	51 (38)	322 (37)	30 (49)	201 (51)	288 (55)	301 (55)
β_{23}	−45 (52)	−36 (23)	22 (56)	15 (51)	−14 (37)	35 (39)	76 (39)	74 (39)

Table 2 (continued)

430 K

	Ca	Ti	Si	01	02A	02B	03A	03B
x	0.2459 (4)	0.5096 (1)	0.7481 (3)	0.7490 (4)	0.9102 (4)	0.0885 (4)	0.3832 (4)	0.6183 (4)
y	0.4187 (1)	0.2530 (1)	0.4328 (1)	0.3207 (2)	0.3160 (3)	0.1839 (3)	0.4603 (3)	0.0398 (3)
z	0.2515 (3)	0.7497 (1)	0.2489 (4)	0.7488 (6)	0.4342 (5)	0.0642 (5)	0.6468 (5)	0.8528 (5)
β_{11}	1387 (18)	618 (9)	288 (14)	382 (33)	698 (47)	760 (48)	631 (46)	615 (44)
β_{22}	198 (6)	206 (5)	113 (7)	252 (17)	307 (32)	339 (32)	231 (28)	208 (27)
β_{33}	527 (12)	364 (8)	222 (14)	929 (38)	455 (84)	354 (82)	741 (82)	494 (75)
β_{12}	17 (18)	58 (7)	−13 (17)	−56 (38)	6 (33)	74 (34)	115 (33)	45 (32)
β_{13}	−76 (11)	115 (7)	63 (12)	314 (31)	70 (48)	156 (49)	351 (51)	226 (47)
β_{23}	−30 (19)	−3 (7)	−25 (21)	−68 (54)	−55 (41)	113 (40)	149 (43)	−23 (41)

440 K

	Ca	Ti	Si	01	02A	02B	03A	03B
x	0.2468 (8)	0.5061 (3)	0.7504 (9)	0.7467 (9)	0.9118 (8)	0.0901 (8)	0.3816 (17)	0.6170 (7)
y	0.4187 (1)	0.2511 (5)	0.4326 (1)	0.3204 (3)	0.3175 (9)	0.1849 (9)	0.4591 (9)	0.0385 (8)
z	0.2535 (12)	0.7509 (6)	0.2491 (15)	0.7450 (17)	0.4351 (11)	0.0660 (11)	0.6458 (11)	0.8517 (10)
β_{11}	1501 (27)	715 (14)	345 (19)	499 (48)	715 (92)	753 (92)	606 (53)	733 (59)
β_{22}	223 (8)	242 (7)	131 (9)	263 (23)	352 (130)	353 (115)	297 (31)	158 (32)
β_{33}	500 (24)	381 (11)	223 (20)	1049 (64)	437 (184)	626 (194)	698 (41)	533 (58)
β_{12}	168 (49)	97 (11)	−185 (38)	−106 (86)	24 (73)	119 (70)	35 (38)	138 (41)
β_{13}	−57 (18)	105 (12)	74 (16)	413 (47)	58 (105)	257 (110)	305 (46)	269 (53)
β_{23}	−3 (54)	2 (9)	−31 (51)	−158 (138)	−97 (119)	203 (115)	18 (40)	124 (41)

450 K

	Ca	Ti	Si	01	02A	02B	03A	03B
x	0.2432 (5)	0.5012 (3)	0.7509 (5)	0.7486 (12)	0.9112 (8)	0.0889 (8)	0.3837 (8)	0.6185 (8)
y	0.4186 (1)	0.2515 (3)	0.4328 (1)	0.3210 (2)	0.3155 (7)	0.1834 (7)	0.4600 (5)	0.0391 (6)
z	0.2509 (4)	0.7503 (3)	0.2511 (5)	0.7507 (14)	0.4366 (10)	0.0659 (10)	0.6471 (10)	0.8531 (9)
β_{11}	1455 (27)	766 (13)	307 (18)	498 (46)	670 (103)	875 (109)	462 (107)	814 (109)
β_{22}	225 (7)	230 (6)	129 (9)	285 (23)	483 (74)	235 (68)	53 (67)	499 (90)
β_{33}	595 (17)	402 (11)	251 (19)	966 (53)	186 (106)	657 (22)	1064 (153)	372 (130)
β_{12}	226 (32)	103 (9)	79 (37)	299 (94)	−67 (78)	214 (76)	−127 (64)	347 (73)
β_{13}	−31 (16)	113 (9)	49 (15)	335 (43)	−234 (91)	458 (102)	464 (123)	181 (111)
β_{23}	180 (31)	0 (8)	37 (40)	−5 (118)	13 (77)	72 (79)	372 (68)	573 (74)

500 K

	Ca	Ti	Si	01	02A	02B	03A	03B
x	0.2500	0.5000	0.7500	0.7500	0.9113 (3)		0.3829 (3)	
y	0.6689 (1)	0.5000	0.6827 (1)	0.5703 (3)	0.5658 (2)		0.7108 (2)	
z	0.5000	0.0000	0.5000	0.0000	0.6857 (2)		0.8974 (3)	
β_{11}	1819 (62)	1018 (41)	547 (61)	472 (50)	949 (36)		807 (37)	
β_{22}	317 (25)	324 (19)	164 (29)	301 (26)	396 (20)		274 (19)	
β_{33}	842 (59)	547 (38)	279 (61)	1120 (64)	606 (41)		767 (39)	
β_{12}		90 (39)			93 (25)		96 (24)	
β_{13}	39 (50)	193 (30)	92 (52)	356 (48)	220 (31)		365 (32)	
β_{23}		−47 (39)			20 (23)		121 (23)	

Table 2 (continued)

600 K

	Ca	Ti	Si	01	02A	02B	03A	03B
x	0.2500	0.5000	0.7500	0.7500	0.9104 (3)		0.3828 (3)	
y	0.6690 (1)	0.5000	0.6827 (1)	0.5699 (3)	0.5665 (2)		0.7106 (2)	
z	0.5000	0.0000	0.5000	0.0000	0.6846 (3)		0.8974 (3)	
β_{11}	1952 (75)	915 (46)	486 (69)	657 (64)	951 (43)		767 (44)	
β_{22}	298 (28)	303 (21)	180 (33)	289 (31)	421 (24)		297 (22)	
β_{33}	874 (66)	644 (45)	243 (67)	1281 (77)	567 (48)		912 (47)	
β_{12}		88 (33)			86 (29)		103 (28)	
β_{13}	21 (58)	209 (35)	70 (58)	506 (59)	183 (37)		379 (39)	
β_{23}		−1 (33)			−1 (27)		124 (27)	

700 K

	Ca	Ti	Si	01	02A	02B	03A	03B
x	0.2500	0.5000	0.7500	0.7500	0.9099 (9)		0.3825 (9)	
y	0.6692 (3)	0.5000	0.6819 (3)	0.5699 (9)	0.5677 (6)		0.7090 (6)	
z	0.5000	0.0000	0.5000	0.0000	0.6827 (9)		0.8973 (8)	
β_{11}	1976 (77)	967 (48)	537 (74)	563 (65)	1022 (54)		979 (52)	
β_{22}	412 (32)	404 (24)	220 (35)	399 (34)	504 (25)		341 (25)	
β_{33}	1190 (76)	743 (45)	401 (70)	1387 (84)	797 (53)		1018 (52)	
β_{12}		59 (37)			124 (33)		90 (30)	
β_{13}	117 (64)	246 (37)	124 (63)	394 (64)	239 (44)		505 (47)	
β_{23}		−67 (39)			69 (31)		81 (30)	

distortions associated with the transition can be obtained by using a symmetry approach. From Table 1 of Stokes and Hatch (1988) it can be seen that a transition from a $C2/c$ [2] ($A2/a$) to a $P2_1/c$ [3] ($P2_1/a$) phase can result from the onset of an order parameter from an irreducible representation. Such a change in space group results from the spontaneous onset of either one of two order parameters corresponding to Y_2^+ or Y_2^-. The irreducible representation Y_2^+ satisfies the Landau and Lifshitz conditions. A transition driven by Y_2^+ could be continuous if the microscopic interactions were such that the order parameter grew continuously from zero as the transition was crossed from above. The subgroup $P2_1/c$ results from lost symmetry elements of $C2/c$, and by selecting the orientation of the new axes as (001), (010), ($\bar{1}0\bar{1}$) and the location of the new origin (000), the standard description given in the *International Tables for Crystallography*, v. A (1986) is obtained. The Y_2^- representation has a similar description, where the new axes are the same as those of the higher symmetry phase but an origin shift of (1/4, 1/4, 0) is required. The order parameter for each representation has one component (one dimensional). Even though each order parameter gives the same space group symmetry, they are different order parameters. The distinction between them comes from their transformation properties relative to the higher symmetry space group $C2/c$. This difference demands a difference in the microscopic distortions making up the two order parameters, i.e., the two resulting $P2_1/c$ phases are distinct structures. In the development of our discussion we will show that the correct structure is obtained by the Y_2^+ representation and we will thus develop our discussion only for this representation.

The Y_2^+ representation is one-dimensional and the part of the free energy obtained from the primary order parameter is of the form

$$\Delta F = a\eta^2 + b\eta^4 + c\eta^6$$

to sixth degree. The order parameter η can couple to other secondary order parameters. These secondary order parameters onset at the transition but do not cause a further symmetry reduction. They must be consistent with the symmetry reduction caused by the primary order parameter of Y_2^+ and thus contain $P2_1/c$ as a subgroup. Only one other representation of $C2/c$ satisfies this condition, namely, Γ_1^+. This representation is symmetry preserving, i.e., the onset of a Γ_1^+ order parameter does not change the symmetry from $C2/c$. Denoting this single component secondary order parameter as ψ, the free energy including both order parameters is

$$\Delta F = a_1\eta^2 + b\eta^4 + c\eta^6 + a_2\psi^2 + \lambda\psi\eta^2,$$

where we have ignored higher order terms in ψ since they are expected to be negligible. Here a_1, b, c, a_2, and λ are constants.

[2] The first setting in the International Tables of the monoclinic space groups are used by Stokes and Hatch (1988) with the unique axis b

[3] See footnote 2

Table 3

a. Titanite, $CaTiSiO_5$: Interatomic distances (Å) as a function of temperature

	294 K	350 K	400 K	430 K	440 K	450 K	500 K	600 K	700 K
Ti–01	1.770 (3)	1.774 (3)	1.784 (3)	1.798 (3)	1.820 (7)	1.850 (7)	1.872 (1)	1.871 (1)	1.876 (1)
Ti–01′	1.983 (3)	1.977 (3)	1.965 (3)	1.949 (3)	1.924 (7)	1.897 (7)	1.872 (1)	1.871 (1)	1.876 (1)
Ti–02A	1.999 (3)	1.991 (3)	1.993 (3)	1.994 (3)	1.999 (8)	1.986 (6)	1.989 (2)	1.998 (2)	2.000 (2)
Ti–02B	1.989 (3)	1.986 (3)	1.986 (3)	1.990 (4)	1.991 (8)	1.994 (7)	1.989 (2)	1.998 (2)	2.000 (2)
Ti–03A	2.019 (3)	2.021 (3)	2.017 (3)	2.016 (3)	2.016 (8)	2.005 (6)	2.023 (2)	2.022 (2)	2.024 (2)
Ti–03B	2.026 (3)	2.025 (3)	2.026 (3)	2.024 (3)	2.022 (8)	2.036 (6)	2.023 (2)	2.022 (2)	2.024 (2)
Mean	1.964	1.962	1.962	1.962	1.962	1.961	1.961	1.964	1.967
Ca–01	2.267 (2)	2.273 (2)	2.273 (2)	2.276 (2)	2.281 (3)	2.277 (2)	2.281 (3)	2.285 (3)	2.272 (4)
Ca–02A	2.426 (3)	2.429 (3)	2.428 (3)	2.429 (4)	2.434 (8)	2.434 (6)	2.426 (2)	2.429 (2)	2.432 (3)
Ca–02B	2.402 (3)	2.408 (3)	2.411 (3)	2.412 (4)	2.413 (8)	2.415 (6)	2.426 (2)	2.429 (2)	2.432 (3)
Ca–03A	2.399 (3)	2.403 (3)	2.407 (4)	2.414 (4)	2.388 (10)	2.412 (7)	2.423 (2)	2.425 (2)	2.431 (3)
Ca–03B	2.424 (3)	2.429 (3)	2.431 (4)	2.425 (4)	2.451 (10)	2.429 (6)	2.423 (2)	2.425 (2)	2.431 (3)
Ca–03A′	2.674 (3)	2.670 (3)	2.665 (3)	2.661 (4)	2.660 (7)	2.667 (6)	2.625 (2)	2.626 (2)	2.630 (3)
Ca–03B′	2.589 (3)	2.593 (3)	2.595 (3)	2.598 (4)	2.600 (7)	2.590 (6)	2.625 (2)	2.626 (2)	2.630 (3)
Mean	2.454	2.458	2.459	2.459	2.461	2.461	2.461	2.464	2.465
Si–02A	1.639 (3)	1.647 (3)	1.644 (3)	1.639 (4)	1.639 (9)	1.646 (6)	1.649 (2)	1.640 (2)	1.641 (3)
Si–02B	1.643 (3)	1.645 (3)	1.648 (3)	1.646 (4)	1.640 (9)	1.645 (6)	1.649 (2)	1.640 (2)	1.642 (3)
Si–03A	1.650 (3)	1.647 (3)	1.648 (3)	1.647 (4)	1.663 (9)	1.657 (6)	1.648 (2)	1.650 (2)	1.645 (3)
Si–03B	1.648 (3)	1.647 (3)	1.647 (3)	1.647 (4)	1.636 (9)	1.642 (6)	1.648 (2)	1.650 (2)	1.645 (3)
Mean	1.645	1.646	1.647	1.645	1.645	1.648	1.648	1.645	1.643

b. Titanite, $CaTiSiO_5$: Interatomic angles (°) as a function of temperature

	294 K	350 K	400 K	430 K	440 K	450 K	500 K	600 K	700 K
01–Ti–02A	92.9 (1)	92.7 (1)	92.3 (2)	91.7 (2)	90.1 (4)	90.3 (3)	90.1 (1)	90.0 (1)	90.1 (1)
01–Ti–02B	93.4 (1)	93.1 (1)	93.0 (2)	92.5 (2)	92.3 (4)	90.4 (3)	90.1 (1)	90.0 (1)	90.1 (1)
01–Ti–03A	90.2 (1)	89.7 (1)	89.8 (1)	89.5 (2)	88.6 (3)	92.4 (2)	92.3 (1)	92.2 (1)	92.4 (1)
01–Ti–03B	95.2 (1)	94.9 (1)	94.8 (1)	94.3 (2)	94.0 (2)	92.3 (2)	92.3 (1)	92.2 (1)	92.4 (1)
01′–Ti–02A	86.9 (1)	87.1 (1)	87.2 (1)	87.7 (2)	88.0 (4)	89.7 (2)	89.9 (1)	90.0 (1)	89.9 (1)
01′–Ti–02B	86.8 (1)	87.1 (1)	87.5 (1)	88.0 (2)	89.6 (4)	89.5 (3)	89.9 (1)	90.0 (1)	89.9 (1)
01′–Ti–03A	89.7 (1)	90.1 (1)	89.9 (1)	90.2 (1)	90.3 (2)	87.9 (3)	87.7 (1)	87.8 (1)	87.6 (1)
01′–Ti–03B	84.9 (1)	85.3 (1)	85.5 (1)	85.9 (1)	87.0 (2)	87.3 (2)	87.7 (1)	87.8 (1)	87.6 (1)
02A–Ti–03A	89.8 (1)	89.9 (1)	90.0 (1)	90.0 (1)	89.9 (3)	90.1 (3)	90.1 (1)	90.1 (1)	90.3 (1)
02A–Ti–03B	89.9 (1)	89.8 (1)	89.8 (1)	89.8 (1)	89.3 (3)	89.6 (3)	89.9 (1)	89.9 (1)	89.7 (1)
02B–Ti–03A	90.2 (1)	90.0 (1)	90.1 (1)	90.0 (1)	90.5 (3)	90.3 (3)	90.1 (1)	90.1 (1)	90.3 (1)
02B–Ti–03B	90.1 (1)	90.3 (1)	90.1 (1)	90.4 (1)	90.4 (1)	90.2 (3)	90.1 (1)	90.1 (1)	90.3 (1)
Ti–01–Ti	140.9 (1)	141.2 (1)	141.2 (1)	141.4 (1)	141.6 (1)	141.6 (1)	141.6 (1)	141.9 (2)	141.0 (2)
02A–Si–02B	102.9 (2)	103.1 (1)	103.1 (1)	103.2 (2)	103.4 (4)	103.3 (3)	103.3 (1)	103.3 (2)	103.5 (2)
02A–Si–03A	112.5 (2)	112.5 (2)	112.6 (2)	113.0 (2)	112.2 (6)	112.9 (3)	112.7 (1)	112.7 (1)	112.8 (1)
02A–Si–03B	108.2 (2)	108.2 (2)	108.2 (2)	108.4 (2)	108.0 (4)	109.1 (3)	108.4 (1)	108.4 (1)	108.4 (1)
02B–Si–03A	108.9 (2)	108.9 (2)	108.8 (2)	108.6 (2)	108.9 (4)	107.9 (3)	108.4 (1)	108.4 (1)	108.4 (1)
02B–Si–03B	113.0 (2)	113.0 (2)	112.9 (2)	112.6 (2)	113.4 (6)	112.4 (3)	112.7 (1)	112.7 (1)	112.8 (1)
03A–Si–03B	111.1 (1)	111.1 (1)	111.0 (2)	111.0 (2)	110.8 (4)	111.1 (3)	111.2 (1)	111.1 (2)	110.8 (2)

Allowed Microscopic Distortions

A more detailed definition of the primary and secondary order parameter will now be given. The primary order parameter is a physical entity which transforms under the Y_2^+ representation. Since the change in symmetry from $C2/c$ to $P2_1/c$ is a non-ferroic transition (Stokes and Hatch 1988 Table 1) and Y_2^+ is not a zone center representation, no components of strain transform according to the Y_2^+ representation. Thus strain cannot serve as the primary order parameter. The Ti atoms are located at the 4(*d*) Wyckoff positions of $C2/c$ with site symmetry $C_i(\bar{1})$. By inducing a representation (Hatch et al. 1987; Kovalev 1986) of $C2/c$ from the site representations of C_i at (1/4, 1/4, 1/2) it is seen that Y_2^+ allows a displacement of the form (1) (α, β, γ); (2) $(\alpha, -\beta, \gamma)$; (3) $(-\alpha, -\beta, -\gamma)$; and (4) $(-\alpha, \beta, -\gamma)$, where the displacements (1), (2), (3), and (4) are the displacements at the 4(*d*) positions (1/4, 1/4, 1/2), (3/4, 1/4, 0), (3/4, 3/4, 1/2), (1/4, 3/4, 0) respectively and the entries (Δx, Δy, Δz) in the parentheses indicate displacements from the equilibrium 4(*d*) positions of $C2/c$ caused by the transi-

tion to $P2_1/c$. Note that a displacement with components along **a**, **b**, and **c** is allowed by symmetry. Symmetry restricts the relative displacements of the atoms at the 4(*d*) sites as can be seen from the expressions just given. For example, if the atom at (1/4, 1/4, 1/2) is displaced by (α, β, γ) along **a**, **b**, and **c**, then the atom at (3/4, 1/4, 0) is displaced $(\alpha, -\beta, \gamma)$, with α, β, γ in the two expressions having the same values. Thus the component of the atom at (3/4, 1/4, 0) in the **a** direction is the same as that of the atom at (1/4, 1/4, 1/2), etc.

In a similar manner we can describe the displacements of the Ca atoms from their 4(*e*) positions. Y_2^+ allows a displacement of the form (1) $(\alpha, 0, \gamma)$, (2) $(-\alpha, 0, -\gamma)$, (3) $(-\alpha, 0, -\gamma)$, (4) $(\alpha, 0, \gamma)$ at the 4(*e*) positions $(0, y, 1/4)$, $(0, \bar{y}, 3/4)$, $(1/2, y+1/2, 1/4)$, $(1/2, \bar{y}+1/2, 3/4)$ respectively. These values of α and γ are not the same as those discussed for the 4(*d*) positions. Since the Si and O(1) oxygens are also at 4(*e*) sites, their displacements will be of the same form but with different values of α and γ.

The two inequivalent sets of oxygens O(2) and O(3), each at 8(*f*) sites, have Y_2^+ displacements of the form (1) (α, β, γ), (2) $(\alpha, -\beta, \gamma)$, (3) $(-\alpha, -\beta, -\gamma)$, (4) $(-\alpha, \beta, -\gamma)$, (5) $(-\alpha, -\beta, -\gamma)$, (6) $(-\alpha, \beta, -\gamma)$, (7) (α, β, γ), (8) $(\alpha, -\beta, \gamma)$ at the sites (x, y, z), $(\bar{x}, y, \bar{z}+1/2)$, $(\bar{x}, \bar{y}, \bar{z})$, $(x, \bar{y}+1/2)$, $(x+1/2, y+1/2, z)$, $(\bar{x}+1/2, y+1/2, \bar{z}+1/2)$, $(\bar{x}+1/2, \bar{y}+1/2, \bar{z})$, $(x+1/2, \bar{y}+1/2, z+1/2)$ respectively.

All of the displacements described above transform according to Y_2^+. At lowest order coupling, they allow linear-linear coupling amongst themselves and with that approximation any one or all can be considered as constituting the primary order parameter. We will take Ti-displacements as the primary order parameter since they are the largest displacements observed experimentally. In the following, the other displacements will be selectively discussed only if they are sizeable and relate to the experimental data obtained.

As can be seen from the free energy form above, the secondary order parameter ψ couples with the primary order parameter η with a linear-quadratic expression respectively. By minimizing ΔF with respect to ψ, i.e., by setting $\dfrac{\partial \Delta F}{\partial \psi}$ equal to zero, the secondary order parameter will depend quadratically on the primary order parameter. The secondary order parameter transforms according to Γ_1^+, which is the same way the strain components ε_{11}, ε_{22}, ε_{33}, and ε_{13} each separately transform (Stokes and Hatch 1988, Table 4). The excess strain which appears at the transition can have only these non-zero components.

As stated earlier, the *x*-ray structure refinements described in this work used the $P2_1/a$ positions given by Taylor and Brown (1976); [0, 1/4, 1/4] added to those values were used for the starting positions of $A2/a$. Up to this point in our development of this section, we have used the $C2/c$ space group given by Stokes and Hatch (1988) as the basis for our discussion. The transformation which takes coordinates in $C2/c$ to those of $A2/a$ consists of two successive steps: (a) The coordinates $(x, y, z)_C$ in $C2/c$ are taken to the coordinates $(z, y, -x+z)_A$ in $A2/a$. This results from the new orientation of axes in $A2/a$, (101) (010) ($\bar{1}$00). (b) An origin shift is made which adds (0, 1/4, −1/4) to those coordinates obtained in (a). Thus the primary order parameter displacements take a slightly different form in $A2/a$. For the 4(*d*) positions of $C2/c$, the correspondence of the two space group descriptions is the following:

	$C2/c$ positions	Displacements	$A2/a$ positions	Displacements
(1)	(1/4, 1/4, 1/2)	(α, β, γ)	(1/2, 1/2, 0)	$(\gamma, \beta, \gamma-\alpha)$
(2)	(3/4, 1/4, 0)	$(\alpha, -\beta, \gamma)$	(0, 1/2, 0)	$(\gamma, -\beta, \gamma-\alpha)$
(3)	(3/4, 3/4, 1/2)	$(-\alpha, -\beta, -\gamma)$	(1/2, 0, 1/2)	$(-\gamma, -\beta, -\gamma+\alpha)$
(4)	(1/4, 3/4, 0)	$(-\alpha, \beta, -\gamma)$	(0, 0, 1/2)	$(-\gamma, \beta, -\gamma+\alpha)$

For the 4(*e*) positions of $C2/c$ the correspondence is:

	$C2/c$ positions	Displacements	$A2/a$ positions	Displacements
(1)	$(0, y, 1/4)$	$(\alpha, 0, \gamma)$	$(1/4, y+1/4, 0)$	$(\gamma, 0, \gamma-\alpha)$
(2)	$(0, \bar{y}, 3/4)$	$(-\alpha, 0, -\gamma)$	$(3/4, \bar{y}+1/4, 1/2)$	$(-\gamma, 0, -\gamma+\alpha)$
(3)	$(1/2, y+1/2, 1/4)$	$(-\alpha, 0, -\gamma)$	$(1/4, y+3/4, 1/2)$	$(-\gamma, 0, -\gamma+\alpha)$
(4)	$(1/2, \bar{y}+1/2, 3/4)$	$(\alpha, 0, \gamma)$	$(3/4, \bar{y}+3/4, 0)$	$(\gamma, 0, \gamma-\alpha)$

The independent strain components ε_{11}, ε_{22}, ε_{33}, and ε_{13} in $C2/c$ give the same independent forms for spontaneous strain in the $A2/a$ space group setting.

Coupling of the Order Parameter with Spontaneous Strain

The spontaneous strain is defined as the strain associated with the phase transition rather than due to thermal expansion. To describe the spontaneous strain, where both the high temperature and low temperature phases are monoclinic, we define an orthogonal coordinate system *x*, *y*, *z*, such that *x* is parallel to **a***, *y* is parallel to **b**, and *z* is parallel to **c**. The spontaneous strain components ε_{ij} (see Schlenker et al. 1978; Ohashi and Burnham 1973) are:

$$\varepsilon_{11} = \frac{a \sin\beta}{a_0 \sin\beta_0} - 1,$$

$$\varepsilon_{22} = \frac{b}{b_0} - 1,$$

$$\varepsilon_{33} = \frac{c}{c_0} - 1,$$

$$\varepsilon_{13} = \frac{1}{2}\left[\frac{a\cos\beta}{a_0 \sin\beta_0} - \frac{c\cos\beta_0}{c_0 \sin\beta_0}\right],$$

$$\varepsilon_{12} = \varepsilon_{23} = 0.$$

Because of the much higher level of precision, the spontaneous strain components have been calculated from the averaged unit cell dimensions at each temperature used for *x*-ray intensity data collection and structure refine-

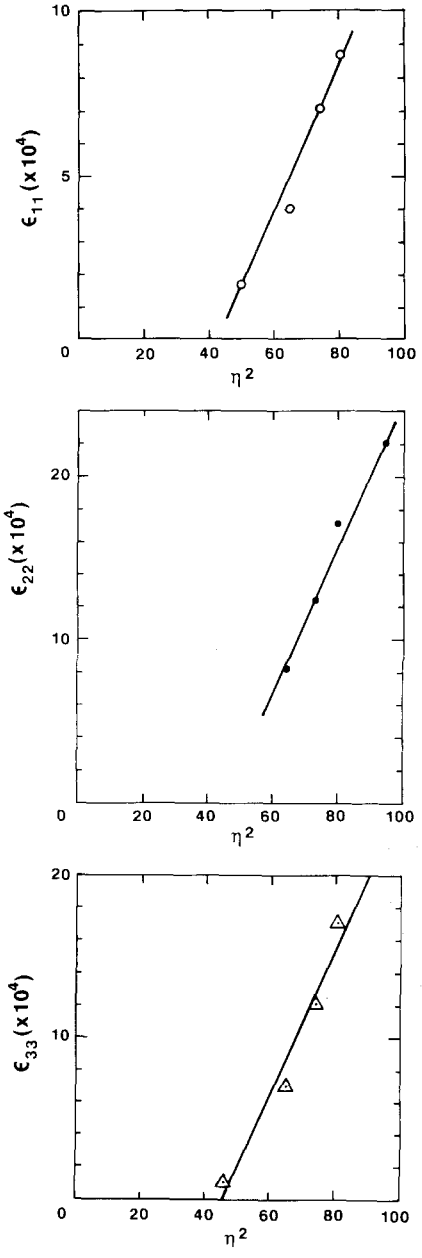

Fig. 4. The strain components, ε_{ii} vs. the squares of the Ti displacements

ment (Table 1). As can be seen from Fig. 4, the strain associated with the phase transition is relatively small. The components ε_{22} and ε_{33} are nearly equal in magnitude, whereas ε_{11} is significantly smaller, and ε_{13} is negligible. The smaller ε_{11} component presumably results from the Ti- and Ca-displacements parallel and antiparallel to **a** and the relative inflexibility of the structure along this direction.

The strain components ε_{11}, ε_{22}, and ε_{33} which transform as the Γ_1^+ representation show a linear relationship with η^2, where η is given by the magnitude of the Ti-displacement (Fig. 4). Hence, $\varepsilon_{ij} \propto \eta^2$. This is consistent with the symmetry analysis given above for the lowest order expansions of the Landau free energy.

Thermal Dependence of Superstructure Reflections

Measurement of the intensities and line-widths of three strong superstructure reflections ($k+l=$ odd): (401), (801), and ($\bar{4}01$) shows a remarkable change in behavior during the first cycle of heating and cooling (Fig. 5). On heating, the thermal dependence of the intensities shows a T_c of 495 ± 5 K with no residual intensities above T_c. In contrast, on cooling T_c is lowered to 445 ± 5 K and residual (diffuse) intensities are observable up to 475 K. Furthermore, the line-widths remain constant up to T_c (495 K) on heating; on cooling from above T_c the line-widths decrease as $T \rightarrow T_c$ and then remain constant down to 294 K. Notice that the constant line-width below T_c observed on cooling is considerably larger than that observed on heating (Fig. 5). These differences in behavior disappear on heating in the second cycle, where the behavior is the same as that observed on cooling during the first cycle. In addition to these effects, a significant decrease in the intensities has been observed in the 294–350 K range both on heating and cooling indicating some structural relaxation. However, we have not investigated the structural details of this effect.

Ti-Displacement as the Primary Order Parameter

As mentioned earlier, the Ti-displacement from the center of the [TiO_6] octahedron has been taken as the primary order parameter, η, which drives the phase transition. Because the Ti position in the $A2/a$ phase is fixed by symmetry, the Ti-displacements in the low temperature ($P2_1/a$) phase from this position can be determined very precisely. Since the displacements are primarily along **a**, the precision essentially depends on the precision of the x coordinate of the Ti position in the $P2_1/a$ phase (Table 2). Even at 450 K (5 K beyond T_c), the Ti displacement [0.8 (2) Å $\times 10^{-2}$] has a statistically significant non-zero value in spite of the fact that the largest root-mean-square displacement due to anisotropic thermal vibration is ± 0.135 Å at this temperature. The Ti displacement plotted as a function of temperature is shown in Fig. 6, which shows a typical second-order behavior; it decreases from 9.76 Å ($\times 10^{-2}$) at 294 K to a near-zero value at T_c (445 K). The fact that slightly above T_c (450 K) it still retains a small non-zero value is consistent with the observed residual intensity of the superstructure reflections. Both sets of observations indicate the presence of precursor clusters with the symmetry of the low temperature phase immediately above T_c. Presence of such precursor clusters above T_c have been observed previously for the $P2_1/a \rightarrow Pnam$ transition in ilvaite, $Ca(Fe^{2+}, Fe^{3+})Fe^{2+}Si_2O_8(OH)$ (Ghose et al. 1989) and the $P\bar{1} \rightarrow I\bar{1}$ transition in anorthite, $CaAl_2Si_2O_8$ (Ghose et al. 1988; Van Tendeloo et al. 1989).

The Ti-displacements are essentially parallel and antiparallel to **a**. In the high temperature ($A2/a$) phase, the titanium atoms occur in the 4(b) positions: (0, 1/2, 0); (1/2, 1/2, 0); (0, 0, 1/2), and (1/2, 0, 1/2), which we designate as 1, 2, 3, and 4, respectively. The corresponding

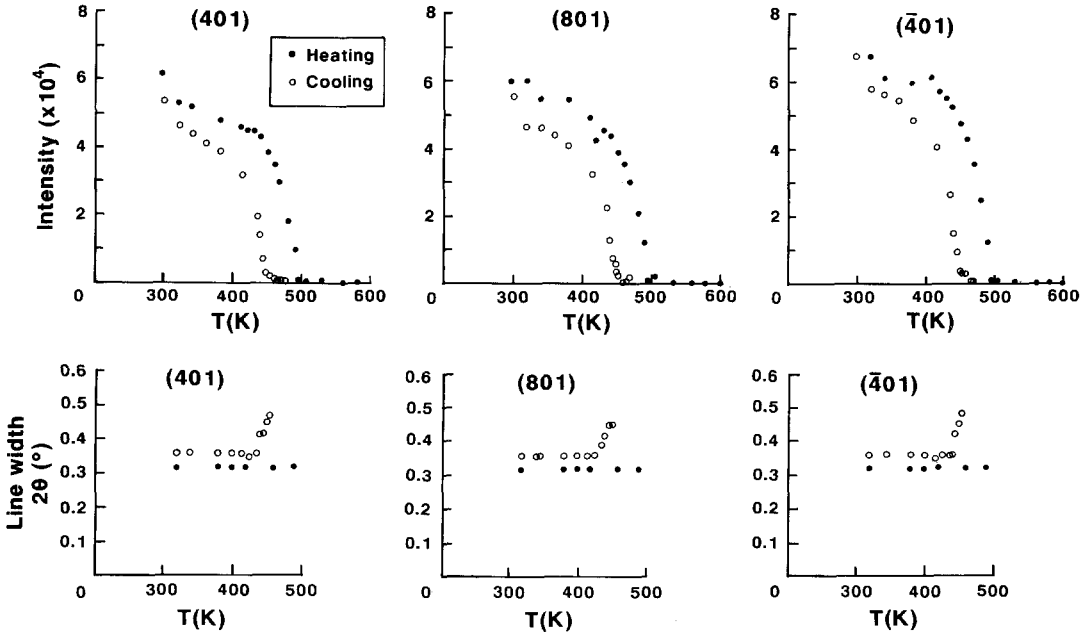

Fig. 5. Thermal dependence of the internsities and line-widths of superstructure reflections (401), (801), and ($\bar{4}01$) on heating (●) and cooling (○) during the first cycle

4(*e*) positions in the low-temperature ($P2_1/a$) phase, obtained by subtracting (0, 1/4, 1/4) for the 4(*b*) positions in $A2/a$, are given by (1) (x, y, z); (2) ($\bar{x}, \bar{y}, \bar{z}$); (3) ($1/2-x$, $1/2+y, \bar{z}$), and (4) ($1/2+x$, $1/2-y, z$). The correspondence between the two sets of positions and the sense of the Ti-displacements parallel (+) and antiparallel (−) to **a** from the 4(*b*) position of $A2/a$ are given below:

$A2/a$ 4(*b*)	$P2_1/a$ 4(*e*)	Ti-Displacement
1	4	+
2	1	+
3	3	−
4	2	−

The experimentally observed Ti-displacements are exactly those predicted by the induced representation theory given above. Notice that the order of the 4(*b*) positions used here is different from the order given earlier. The relative displacements from positions related by the *A*-centering, i.e., 1 and 3 on the one hand, and 2 and 4 on the other, have equal and opposite displacements.

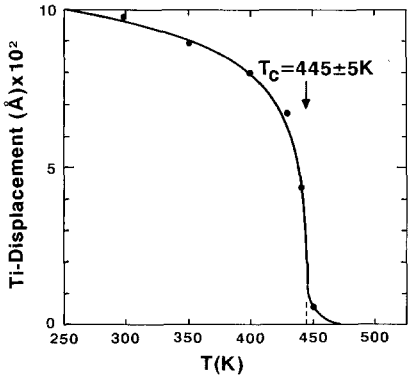

Fig. 6. Ti-displacements as a function of temperature. Note the small non-zero value above T_c (445 K)

The other significant atomic displacement involves the Ca atoms, which occur in the 4(*e*) position of $A2/a$: (1) (1/4, y, 0); (2) (3/4, $\bar{y}$, 0); (3) (1/4, $1/2+y$, 1/2); and (4) (3/4, $1/2-y$, 1/2). After subtracting (0, 1/4, 1/4), these positions correspond to the 4(*e*) positions in $P2_1/a$: (1) (x, y, z); (2) ($\bar{x}, \bar{y}, \bar{z}$); (3) ($1/2-x$, $1/2+y, \bar{z}$); and (4) ($1/2+x$, $1/2-y, z$) in the following way:

$A2/a$ 4(*e*)	$P2_1/a$ 4(*e*)	Ca-Displacement
1	3	+
2	2	+
3	1	−
4	4	−

The Ca-displacements are also essentially parallel (+) and antiparallel (−) to **a** (cf. Taylor and Brown 1976) and the nearest Ca and Ti atoms are displaced in the same sense. Again, the observed Ca-displacements are in agreement with those predicted by the induced representation theory. As in the case of Ti-displacements, the Ca displacements related by the *A*-centering are equal and opposite to each other. The Ca-displacements are considerably smaller than the Ti-displacements with a value of 5.59 (Å) ($\times 10^{-2}$) at 294 K attaining a near-zero value at T_c. The Ca- and Ti-displacements determined at any given temperature are plotted in Fig. 7, which shows a linear relationship as expected from the lowest order coupling obtained from symmetry considerations.

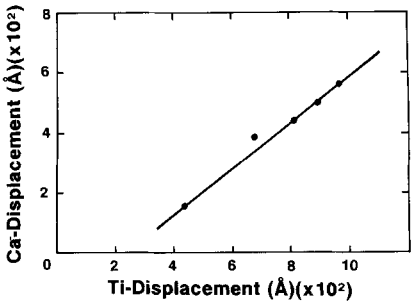

Fig. 7. Ti-displacement vs. Ca-displacement at any given temperature

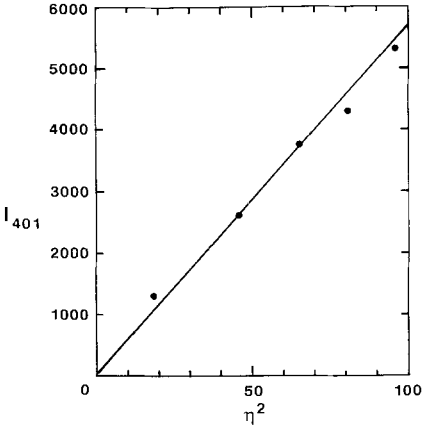

Fig. 8. Intensity of the superstructure reflection (401) vs. the square of Ti-displacement

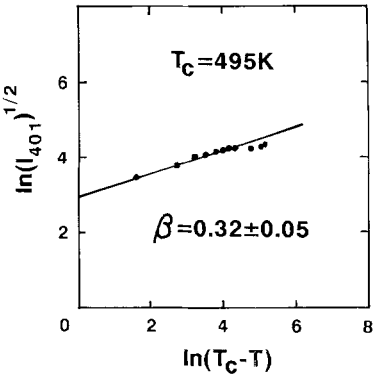

Fig. 9. A plot of $\ln(I_{401})^{1/2}$ vs. $\ln(T_c - T)$. The critical exponent, $\beta = 0.32 \pm 0.05$

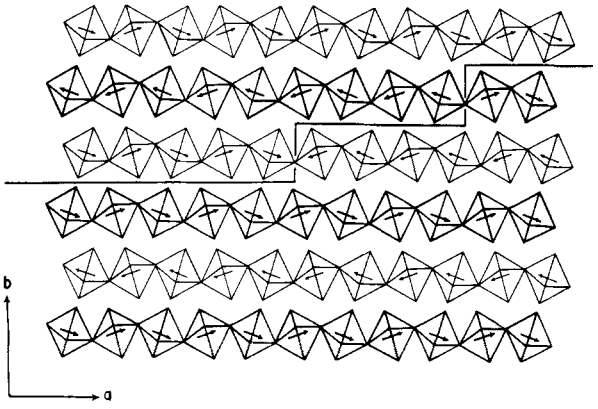

Fig. 10. A schematic view of the antiphase domain structure in titanite. Dark and light outlines represent Ti octahedral chains above and below the plane of the drawing. The arrows represent Ti displacements. The heavy stepped line in the middle shows a domain boundary (after Taylor and Brown 1976)

Critical Exponent of the Order Parameter

The squares of the Ti-displacements plotted against the intensities of the superstructure reflection (401) show a linear relationship, indicating $I \propto \eta^2$ (Fig. 8). Since the direct measurement of the order parameter, η, from Ti-displacements have been made only at few temperatures, we have determined the critical exponent, β, from the intensities of superstructure reflections. The critical exponent, β is related to η as:

$$\eta = \eta_0 (T_c - T)^{\beta}.$$

A plot of $\ln(I_{401})^{1/2}$ vs. $\ln(T_c - T)$ yields a value of 0.32 $\pm$0.05 (Fig. 9), which is remarkably close to the value of 1/3. This value of the critical exponent indicates a three dimensional Ising behavior rather than the mean-field behavior near T_c, since the predicted critical exponent from the mean-field theory (Landau theory) is either 1/2, or 1/4 if the transition is close to a tricritical point.

Thermal Dependence and Unpinning of Antiphase Domain Boundaries

The $A2/a$ to $P2_1/a$ phase transition involves a loss of the translational symmetry [0, 1/2, 1/2] only and no loss of point symmetry. This implies that following the transition, the low temperature phase will show antiphase domains with a displacement vector, $\mathbf{R} = [0, 1/2, 1/2]$. From the x-ray and electron diffraction evidence, such antiphase domains have been postulated by previous workers (Speer and Gibbs 1976; Taylor and Brown 1976; Higgins and Ribbe 1976). The nature of the antiphase domains to be expected is schematically shown in Fig. 10. Higgins and Ribbe (1976) observed diffuse sheets parallel to (100) in electron diffraction patterns at the positions of $(k+l)$ odd reflections at room temperature in a natural titanite and concluded that the antiphase domains are linear and parallel to a. Such antiphase domains can be imaged directly by the transmission electron microscope (TEM) in the dark field. The high temperature TEM experiments on titanite are currently in progress. In the meantime, we can make certain predictions with regard to the thermal behavior of the antiphase domains from the temperature dependence of intensities and line-widths of superstructure reflections observed by x-ray diffraction. Since the line-width of a su-

perstructure reflection is given by the Fourier transform of the antiphase domain size and shape (see Hamil et al. 1975), the line-width and domain size are inversely proportional to each other. We recall that on heating during the first cycle, the superstructure reflections remain sharp up to T_c (495 K) (Fig. 5). This implies relatively large antiphase domains (>250 Å) with static boundaries, which remain constant up to T_c and disappear abruptly at T_c. On cooling from above T_c, the diffuse reflection sharpens up considerably on approaching T_c; below T_c, the line-width remains constant, but it is considerably larger than the constant width observed during heating. This indicates a considerable reduction in domain size on cooling. The reorientation of the domain boundaries on heating and cooling is most likely caused by a redistribution of vacancies and defects which were pinning the original boundaries. After the boundaries are unpinned during heating in the first cycle, the defects are most probably uniformly distributed and the thermal dependence of the domains becomes reversible on further cooling and heating. This is shown by the line-width, which remains constant up to T_c and increases above T_c and no longer shows any hysteresis. The increasing line-width above T_c implies a break-up of large domains into smaller domains above T_c, the domain size decreasing continuously with increasing temperature. These small domains above T_c have the symmetry of the low temperature phase ($P2_1/a$) and are the precursor clusters in the stability field of the high temperature phase. Although the diffraction experiments are time-averaged and cannot distinguish between static and dynamic domains, the small antiphase domains above T_c almost certainly are dynamic in nature and result from the critical fluctuations near T_c. We have directly observed such dynamic domains above T_c in connection with the $P\bar{1}-I\bar{1}$ transition in anorthite by transmission electron microscopy (Ghose et al. 1988; Van Tendeloo et al. 1989). It is significant that in titanite, the small dynamic domains above T_c could be observed only after unpinning of the original domain boundaries. Hence, defect interaction with temperature plays a crucial rôle in the transition dynamics of the phase transition.

The question raised by Taylor and Brown (1976) whether the titanium position in the high temperature phase represents an average of two or more titanium positions or a single titanium position with a large thermal component in the axial direction of the octahedron can now be settled on the basis of our observations. The presence of precursor clusters and a non-zero order parameter above T_c indicate that the high temperature phase ($A2/a$) is a statistical average of small dynamic ($P2_1/a$) domains with fluctuating domain walls. The critical lattice fluctuations near T_c cause the Ti-displacements related by A-centering to change from $+\mathbf{a}$ to $-\mathbf{a}$ (or *vice versa*), thereby causing the domain walls to move. In this respect, the dynamic characteristics of the phase transition in titanite are very similar to those of the $P\bar{1}-I\bar{1}$ transition in anorthite where the dynamic domains of the low temperature phase above T_c have been imaged directly by TEM (Ghose et al. 1988; Van Tendeloo et al. 1989).

Microscopic Mechanism and Dynamics of the Phase Transition

We are now in a position to describe the microscopic mechanism and the dynamics of the $P2_1/a$ to $A2/a$ transition in titanite. The phase transition is initially driven by the order parameter, η (Ti-displacements), which transforms as the irreducible represtation, Y_2^+. η is linearly coupled to the Ca-displacements. A coupling of Y_2^+ with the Γ_1^+ mode causes a linear-quadratic coupling of η with the spontaneous strain components, ε_{11}, ε_{22}, ε_{33}, and ε_{13}, i.e. $\varepsilon_{ij} \propto \eta^2$. Ti-displacements decrease continuously in magnitude as T approaches T_c from below but retains a small non-zero value at and slightly above T_c. Near T_c, critical lattice fluctuations cause the phase transition to be finally driven by an order-disorder mechanism whereby Ti-displacements related by near A-centering, i.e. $\sim[0, 1/2, 1/2]$ in adjacent small dynamic domains are continuously interchanged between parallel and antiparallel arrangements (Fig. 10). Hence, this is a fluctuation-driven weakly first-order transition. In the region close to T_c, an onset of soliton mobility (i.e. fluctuation of domain walls) will be observed. Just above T_c, the high temperature ($A2/a$) phase then is a statistical dynamical average of small dynamic ($P2_1/a$) domains. Above T_c, the domain size (i.e. the correlation length) continuously decreases and the fluctuation frequency of the domain walls increases with increasing temperature. Considerably above T_c, the domain size is so small and the fluctuation frequency so high that individual domains can no longer be distinguished. In this region, the structure may be considered to have the $A2/a$ symmetry, where the titanium atom has an equal probability of being slightly displaced parallel and antiparallel to **a** from the central octahedral position. The $A2/a$ symmetry, however, is still a dynamic average of instantaneous $P2_1/a$ configurations. This is the classic case described by the strongly anharmonic deep double-well potential with hopping between the wells. We suggest that such a transition mechanism for displacive "second-order" phase transitions may be fairly universal.

Acknowledgments. We are indebted to Prof. J.A. Speer, Raleigh, North Carolina, for the titanite sample and Yang Hexiong, University of Washington, for a number of computations. Fruitful discussions on the characteristics of phase transitions in ferroelectrics and antiferroelectrics with Profs. S. Kurtz and L.E. Cross, Pennsylvania State University, are gratefully acknowledged. This research has been supported by the National Science Foundation (EAR 8719638).

References

Bond WL (1951) Making small spheres. Rev Sci Instrum 22:344–345

Brower WS, Robbins CR (1969) Growth of $CaTiSiO_5$ by the Czochralski method. J Crystal Growth 5:233–234

Enck DE, Dommel G (1965) Behavior of the thermal expansion of NaCl at elevated temperatures. J Appl Phys 36:839–844

Franke W, Ghobarkar H (1980) The morphology of titanite grown from aqueous critical solutions. Neues Jahrb Mineral Mh Jg 1980:564–568

Ghose S, Tsukimura K, Hatch DM (1989) Phase transitions in ilvaite, a mixed-valence iron silicate II. A high temperature single crystal x-ray diffraction study and Landau theory of the

monoclinic to orthorhombic phase transition induced by charge delocalization. Phys Chem Minerals 16:483–496
Ghose S, Van Tendeloo G, Amelinckx S (1988) Dynamics of a second order phase Transition: $P\bar{1}-I\bar{1}$ phase transition in anorthite. Science 242:1539–1541
Hamil MM, Ghose S, Sparks RA (1975) Antiphase domains in a lunar pigeonite: determination of the average shape, size and orientation from a measurement of three-dimensional intensity profiles of diffuse ($h+k=$odd) reflections. Acta Crystallogr A31:126–130
Hatch DM, Ghose S (1989) A dynamical model for the $P\bar{1}-I\bar{1}$ phase transition in anorthite, $CaAl_2Si_2O_8$. II. Order parameter treatment. Phys Chem Minerals 16:614–620
Hatch DM, Stokes HT, Putnam RM (1987) Symmetry analysis of the microstructure and phase transitions of a crystallographic space group: Applications. Phys Rev B35:4935–4942
Higgins JB, Ribbe PH (1976) The crystal chemistry and space groups of natural and synthetic titanites. Am Mineral 61:878–888
International Tables for X-ray Crystallography (1983) v. A., Reidel, Dordrecht
International Tables for X-ray Crystallography (1974) v. IV. Kynoch Press, Birmingham
Kovalev OV (1986) Irreducible representations of the space groups. Gordon and Breach, New York
Lundgren JO (1982) UPALS, Crystallographic computer programs. University of Uppsala, Uppsala, Sweden
Mongiorgi R, Riva di Sanseverino L (1968) A reconsideration of the structure of titanite, $CaTiOSiO_4$. Mineral Petrogr Acta 14:123–141
Ohashi Y, Burnham CW (1973) Clinopyroxene lattice deformations: The roles of chemical substitution and temperature. Am Mineral 58:843–849
Robbins CR (1968) Synthetic $CaTiSiO_5$ and its germanium analog ($CaTiGeO_5$). Mater Res Bull 3:693–698
Schlenker JL, Gibbs GV, Boisen MB (1978) Strain-tensor components expressed in terms of lattice parameters. Acta Crystallogr A34:52–54
Speer JA, Gibbs GV (1976) The crystal structure of synthetic titanite, $CaTiSiO_5$, and the domain textures of natural titanites. Am Mineral 61:238–247
Stokes HT, Hatch DM (1988) Isotropy subgroups of the 230 crystallographic space groups. Word Scientific, Singapore
Tanaka I, Obuchi T, Kojima H (1988) Growth and characterization of titanite ($CaTiSiO_5$) single crystals by the floating zone method. J Crystal Growth 87:169–174
Taylor M, Brown GE (1976) High temperature structural study of the $P2_1/a \rightleftharpoons A2/a$ phase transition in synthetic titanite, $CaTiSiO_5$. Am Mineral 61:435–447
Tsukimura K, Sato-Sorensen Y, Ghose S (1989) A gas-flow furnace for x-ray crystallography. J Appl Crystallogr 22:401–405
Van Heurck C, Van Tendeloo G, Ghose S, Amelinckx S (1991) Paraelectric-antiferroelectric phase transition in titanite, $CaTiSiO_5$. II. Electron diffraction and electron microscopic studies of the transition dynamics. Phys Chem Minerals 17:604–610
Van Tendeloo G, Ghose S, Amelinckx S (1989) A dynamical model for the $P\bar{1}-I\bar{1}$ phase transition in anorthite, $CaAl_2Si_2O_8$. I. Evidence from electron microscopy. Phys Chem Minerals 16:311–319
Zachariasen WH (1930) The crystal structure of titanite. Zeit Kristallogr 73:7–16

Note added in proof

The structural mechanism of the phase transition proposed in this paper including the mobility of the domain walls has been confirmed by high temperature electron microscopy (Van Heurck et al. 1991).